VIP Solar Energy Conversion Very Important Paper

Deutsche Ausgabe: DOI: 10.1002/ange.201601865
Internationale Ausgabe: DOI: 10.1002/anie.201601865

Integration of Semiconducting Sulfides for Full-Spectrum Solar Energy Absorption and Efficient Charge Separation

Tao-Tao Zhuang[+], Yan Liu[+], Yi Li[+], Yuan Zhao, Liang Wu, Jun Jiang, and Shu-Hong Yu**

Abstract: *The full harvest of solar energy by semiconductors requires a material that simultaneously absorbs across the whole solar spectrum and collects photogenerated electrons and holes separately. The stepwise integration of three semiconducting sulfides, namely ZnS, CdS, and $Cu_{2-x}S$, into a single nanocrystal, led to a unique ternary multi-node sheath ZnS–CdS–$Cu_{2-x}S$ heteronanorod for full-spectrum solar energy absorption. Localized surface plasmon resonance (LSPR) in the nonstoichiometric copper sulfide nanostructures enables effective NIR absorption. More significantly, the construction of pn heterojunctions between $Cu_{2-x}S$ and CdS leads to staggered gaps, as confirmed by first-principles simulations. This band alignment causes effective electron–hole separation in the ternary system and hence enables efficient solar energy conversion.*

Solar radiation is by far the most abundant source of clean and sustainable energy. Effectively harvesting solar energy with semiconductor materials for the production of other energy forms, such as chemical energy,[1] electricity,[2] and thermal energy,[3] is an ideal tactic to conquer the growing global energy crisis. The solar spectrum includes a small share of ultraviolet (UV) radiation (< 400 nm), which comprises approximately 6.8% of the solar power, whereas the visible (vis) range (400–760 nm) accounts for about 38.9%, and infrared radiation (IR, 760–3000 nm) makes up most of the remaining 54.3%.[4] Thus the design and synthesis of semiconductor materials for the full-spectrum absorption of solar radiation is crucial in the energy conversion field. The combination of several semiconductors with diverse band gaps within a single nanocrystal is one promising strategy to achieve this goal.

Among all types of inorganic semiconductors, metal sulfides have been particularly extensively investigated in recent years because of their wide band gaps, which render them good candidates for solar energy conversion.[5] For instance, ZnS is a frequently used material that absorbs in the UV range with a band gap of approximately 3.6 eV,[6] whereas CdS absorbs in the visible range owing to its band gap of about 2.4 eV.[7] By combining ZnS and CdS, a binary ZnS–CdS heteronanorod was obtained that absorbs across the UV and visible range.[8] To further explore the full spectrum of solar energy, some nanosulfides that absorb IR radiation could be incorporated into ZnS–CdS. For example, nonstoichiometric copper sulfide nanocrystals, which show plasmonic absorption in the NIR region because of excess holes in the valence band that are due to copper deficiencies,[9] are attractive candidates for solar-driven applications. Another key issue for solar energy conversion is the effective separation of the photogenerated electrons and holes.[10] Controlling the band alignment through the formation of heterojunctions is a ubiquitous solution for this purpose. Therefore, the development of semiconductors with enhanced solar absorption and efficient charge separation is urgently required, but remains to be a challenge.

Herein, through a colloidal chemical transformation strategy, we constructed a unique ternary sulfide –[ZnS–CdS–$Cu_{2-x}S$]–ZnS– heteronanorod, which features a ZnS nanorod with segmented CdS node sheaths integrated by $Cu_{2-x}S$ sections. The synthesized ternary heteronanorods show an expanded absorption region that spans the UV, visible, and NIR range. More importantly, the selective incorporation of $Cu_{2-x}S$ on CdS domains resulted in a staggered gap alignment owing to the formation of pn heterojunctions between CdS and $Cu_{2-x}S$, as confirmed by first-principles simulations. This ensures the delivery of photogenerated electrons to the conduction band of CdS in such a ternary system while collecting the holes of all semiconductor components in the valence band of $Cu_{2-x}S$, promoting the electron–hole carrier separation. This conventional but unique ternary ZnS–CdS–$Cu_{2-x}S$ semiconductor nanosystem, which does not contain any noble metal domains, displays increased absorption of solar radiation and efficient charge separation, leading to an improved performance in solar energy conversion.

The enhanced solar energy absorption and the efficient charge separation are due to the structure of the ternary sulfide ZnS–CdS–$Cu_{2-x}S$ heteronanostructure, in which CdS interfaces with both ZnS and $Cu_{2-x}S$, while $Cu_{2-x}S$ and ZnS are not in direct contact with each other. The band alignment

[*] T. T. Zhuang,[+] Y. Li,[+] L. Wu, Prof. Dr. S. H. Yu
Division of Nanomaterials & Chemistry
Hefei National Laboratory for Physical Sciences at the Microscale
Collaborative Innovation Center of Suzhou Nano Science and Technology, CAS Center for Excellence in Nanoscience
Hefei Science Center of CAS, Department of Chemistry
University of Science and Technology of China
Hefei 230026 (P.R. China)
E-mail: shyu@ustc.edu.cn
Homepage: http://staff.ustc.edu.cn/~yulab/
Y. Liu,[+] Y. Zhao, Prof. Dr. J. Jiang
Hefei National Laboratory for Physical Sciences at Microscale
iChEM (Collaborative Innovation Center of Chemistry for Energy Materials), School of Chemistry and Materials Science
University of Science and Technology of China
Hefei 230026 (P.R. China)
E-mail: jiangj1@ustc.edu.cn
[+] These authors contributed equally to this work.
Supporting information and the ORCID identification number(s) for the author(s) of this article can be found under http://dx.doi.org/10.1002/anie.201601865.

and the flow of electrons and holes generated by solar irradiation of the hybrid system are illustrated in Scheme 1. Almost the full spectrum of solar radiation, including the UV, visible, and NIR range, can be utilized to form electron–hole pairs. CdS is an n-type semiconductor, whereas $Cu_{2-x}S$ is a

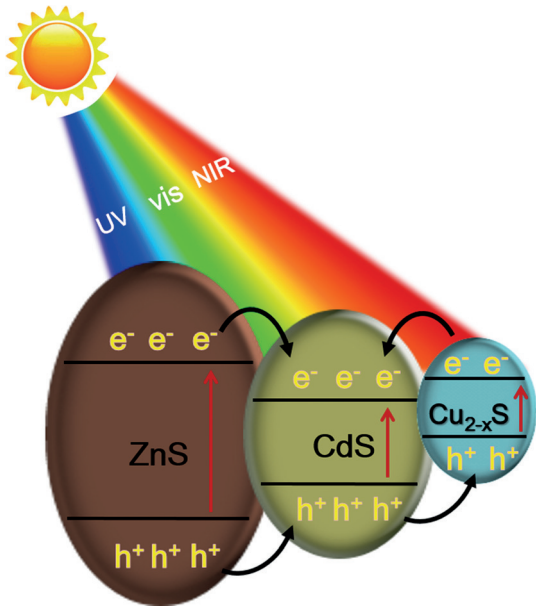

Scheme 1. Energy band alignment and the flow of photogenerated carriers in the ZnS–CdS–$Cu_{2-x}S$ nanosystem. The ZnS–CdS–$Cu_{2-x}S$ ternary hybrid material effectively absorbs UV, visible, and NIR light. The photogenerated electrons flow to the conduction band of CdS in this hybrid system while the hole carriers mostly accumulate at the valence band of $Cu_{2-x}S$.

p-type semiconductor.[11] The band of $Cu_{2-x}S$ is embedded within that of CdS (Supporting Information, Figure S1 a). The contact between $Cu_{2-x}S$ and CdS leads to the formation of a pn junction,[2a,12] and the Fermi level difference thus drives the flow of electrons from CdS to $Cu_{2-x}S$ while holes flow from $Cu_{2-x}S$ to CdS; the two Fermi levels are thus shifted until they reach equilibrium. The pn junction between CdS and $Cu_{2-x}S$ corresponds to a type II heterojunction (Figure S1 b). The stepwise integration of ZnS, CdS, and $Cu_{2-x}S$ will lead to a double heterojunction, resulting in the separate accumulation of electrons and holes (Scheme 1).

To realize the proposed strategy, we synthesized ternary multi-node sheath –[ZnS–CdS–$Cu_{2-x}S$]–ZnS– heteronanorods with segmented CdS node sheaths integrated by $Cu_{2-x}S$ sections. The structural evolution process of the preparation of ZnS–CdS–$Cu_{2-x}S$ is shown in Figure 1 a. The initial reactant, binary node-sheath ZnS–CdS heteronanorods, was prepared by our previously reported colloidal sequential cation exchange procedure (for details see the Supporting Information). The third component, $Cu_{2-x}S$, can be formed only on the CdS node sheaths of ZnS–CdS by a selective partial chemical transformation at room temperature, which enables the construction of ternary ZnS–CdS–$Cu_{2-x}S$ heteronanorods. A cation exchange process, in which the cations of a nanocrystal host lattice are substituted with other cations in

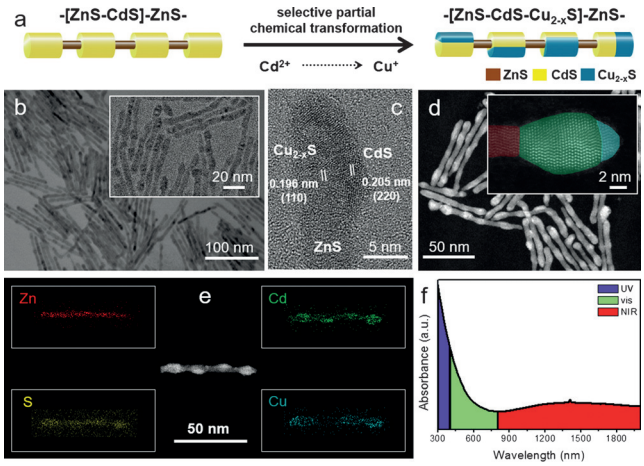

Figure 1. a) Synthesis of ternary ZnS–CdS–$Cu_{2-x}S$ from binary ZnS–CdS by partial cation exchange at room temperature. b) TEM image of ZnS–CdS–$Cu_{2-x}S$. Inset: Magnified TEM image. c) HRTEM image of ZnS–CdS–$Cu_{2-x}S$. d) HAADF-STEM image of the heteronanorods. Inset: High-resolution HAADF-STEM image. ZnS red, CdS green, $Cu_{2-x}S$ cyan. e) EDS mapping images show the segmented node-sheath structure, revealing that $Cu_{2-x}S$ grows only on the CdS node sheaths. f) Absorption spectrum of colloidal ternary ZnS–CdS–$Cu_{2-x}S$ heteronanorods, demonstrating that they absorb across the UV, visible, and NIR range.

solution, constitutes a powerful method for accessing novel nanomaterials. Furthermore, partial cation exchange strategies are particularly versatile for the synthesis of heterostructured ionic nanocrystals, which is significantly expanded here for integrating ternary sulfides. To a first approximation, cation solvation and phase stability can dictate the thermodynamic feasibility of an exchange reaction. The transformation of binary ZnS–CdS into ternary ZnS–CdS–$Cu_{2-x}S$ is favored by the addition of an appropriate amount of Cu^+ in methanol solution. This can be qualitatively understood in terms of the hard/soft acid/base theory,[13] which tabulates the interaction of cations within solvents of varying chemical hardness, η, as a function of their polarizability.[14] Divalent Cd^{2+}, a hard acid ($\eta = 10.29$ eV), in a sulfide host lattice, can be replaced by soft Cu^+ ($\eta = 6.28$ eV) by preferential ligation to polar methanol (a hard base).[13a] Incomplete exchange between Cd^{2+} and Cu^+ in the ZnS–CdS heteronanorods by using a substoichiometric amount of Cu precursor leads to the formation of ZnS—CdS–$Cu_{2-x}S$ (see Figure 1 b). In fact, divalent Zn^{2+} ($\eta = 10.88$ eV) is also a hard acid and can be substituted by Cu^+ in polar solvents.[15] ZnS nanorods can also be partially transformed into copper sulfide (Figure S2), demonstrating that the cation exchange between Zn^{2+} and Cu^+ can also occur when only ZnS is present. In the binary ZnS–CdS hybrid system, more surface defects in the CdS node sheaths, which result from the synthetic method (i.e., sequential cation exchange), may provide plenty of vacancy sites, promoting the selective exchange of Cu^+ in the CdS domains.

Electron microscopy images of a ternary ZnS–CdS–$Cu_{2-x}S$ sample prepared by partial cation exchange are shown in Figure 1 b–e. The transmission electron microscopy (TEM) and high-resolution transmission electron microscopy

(HRTEM) images in Figure 1b,c reveal the morphology of the synthesized ternary product, which adopts the shape of node-sheath heteronanorods, in analogy to that of the binary ZnS–CdS starting material (Figure S3a). The retention of the node-sheath shape was attributed to the large size of the CdS regions relative to the reaction zone. Therefore, only a small portion of the crystallite undergoes structural distortions during the exchange reaction while the remainder of the lattice remains intact.[16] The structural characteristics of the segmented node-sheath heteronanorods were further analyzed by high-angle annular dark field scanning transmission electron microscopy (HAADF-STEM; Figure 1d), showing the contrast between the node sheath (brighter) and the stem. Energy-dispersive X-ray spectroscopy (EDS) mapping was applied to clarify the composition profile of the ternary ZnS–CdS–$Cu_{2-x}S$ compound. As shown in Figure 1e, Zn and S atoms are distributed over the whole rod, while Cd and Cu are present in a segmented manner. The distribution of Cu confirmed that selective partial cation exchange had occurred upon adding Cu^+ precursors to the ZnS–CdS nanosystem. The EDS spectrum of the ternary heteronanorod also reflected the molar ratio of Zn, Cd, and Cu (Figure S4). Compared with the absorption of ZnS–CdS (Figure S3b), the discernible absorption of the as-prepared ternary heteronanorods in the NIR region (Figure 1f) clearly demonstrates the formation of nonstoichiometric copper sulfide ($Cu_{2-x}S$) nanostructures. The observed NIR absorbance originates from localized surface plasmon resonance (LSPR), which is induced by free holes in the valence band of the copper sulfide. The LSPR effect was further manifested by three-dimensional numerical simulations with the finite-element method. We obtained the LSPR frequency ω_{sp} (0.88 eV) and the line width γ (0.5 eV) by fitting to a Gaussian function (Figure S5a; see the Supporting Information for details). Based on these results, we simulated the 2D distribution of the LSPR electric field intensity upon illumination of the $Cu_{2-x}S$ nanocrystal centered in the simulation setup with light of various wavelengths (900, 1000, 1100, 1200, 1300, 1400, 1500, 1600, 1700, and 1800 nm; Figure S5b). As shown in Figure 2, the electric field intensities are much stronger for 1300 nm and 1400 nm irradiation than for other incident wavelengths, indicating the LSPR peak to be located around 1300–1400 nm, which is consistent with the experimental absorption spectra in general. Owing to the LSPR effect, the nanocrystals show intense light absorption and scattering. The integration of ZnS, CdS, and $Cu_{2-x}S$ thus enhances the absorption in various regions, including the UV, visible, and NIR range (Figure S6).

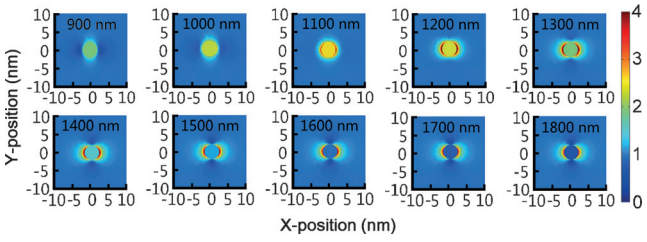

Figure 2. Simulation of the LSPR of $Cu_{2-x}S$ nanocrystals. 2D contour maps of the electric field intensities around the $Cu_{2-x}S$ nanocrystal upon illumination at various wavelengths.

As demonstrated in Figure S7, the XPS spectra used to determine the surface composition distinctly display the fine-scanned S 2p, Zn 2p, Cd 3d, and Cu 2p peaks, and thus also reflect the occurrence of cation exchange and the formation of copper sulfide nanocrystals. The Cu XPS spectrum (Figure S7e) has a weak asymmetric tail, as reported for covellite, which is due to the kinetic energy losses in the reciprocity between photoelectrons and free hole carriers.[17] This result further demonstrates that the copper sulfide in our synthesized ternary heteronanorods is nonstoichiometric, which leads to NIR absorption according to the LSPR effect. A more detailed study of the cation exchange reaction was performed to obtain the exact structure of ternary ZnS–CdS–$Cu_{2-x}S$. The amount of copper sulfide in the ternary hybrid system can be regulated by adding a certain amount of the Cu^+ precursor. At low Cu^+ concentrations, only a small part of CdS is transformed into $Cu_{2-x}S$, which leads to the formation of CdS–$Cu_{2-x}S$ dimers (Cu/Cd = 0.6:0.7, in theory; see Figure S8a). As the exchange of Cd^{2+} is enhanced by the addition of Cu^+, the amount of copper sulfide generated increases (Figure S8b). At even higher Cu^+ concentrations, the entire CdS node sheath is replaced by copper sulfide (Figure S8c). The XRD patterns of ternary heteronanorods prepared with increasing amounts of Cu^+ are shown in Figure S9a. The peaks of the CdS phase gradually disappear, and the peaks belonging to $Cu_{2-x}S$ increase in intensity when the amount of the Cu precursor in the initial reaction is increased. The enhanced NIR absorption in these samples also indicates the increasing amount of copper sulfide in the ternary heteronanorods (Figure S9b). We further used various binary ZnS–CdS heteronanorods with adjustable Zn/Cd molar ratios as reactants (e.g., 1:1, 1:2, and 1:3), and consequently, the structure of the node-sheath heteronanorod can also be retained in the corresponding ternary ZnS–CdS–$Cu_{2-x}S$ products (Figure S10).

On the basis of the experimental and theoretical LSPR analysis above, our ternary ZnS–CdS–$Cu_{2-x}S$ heteronanorod clearly displays nearly full-spectrum absorption (UV, visible, and NIR), thus enhancing the use of solar energy. To analyze the suitability of the ternary sulfide heteronanorod for the separation of photogenerated charges and holes, which limits the efficiency of light conversion, density functional theory (DFT) was utilized to study the band gap alignment of this hybrid material. As the CdS component actually achieved good coupling with the copper sulfide moieties in our experiments, we used pure Cu_2S to model their interface. Indeed, the interaction between ZnS and CdS is weak because they are both n-type semiconductors. Thus we only need to investigate the pn junction in this hybrid, which is composed of CdS (n-type) and Cu_2S (p-type). Based on the optimized unit cells of ZnS, CdS, and Cu_2S, the densities of states were calculated first (Figure S11). The band gap obtained in our simulations is generally consistent with the reported experimental results, confirming the reliability of our calculations (Figure S12). In our ternary system, ZnS and CdS grow along the [111] direction, and the side facet of CdS should be (−110) in contact with Cu_2S(−110). We then simulated the CdS-(−110)/Cu_2S(−110) heterojunction to characterize their interface (Figure 3a). The calculations revealed that the work

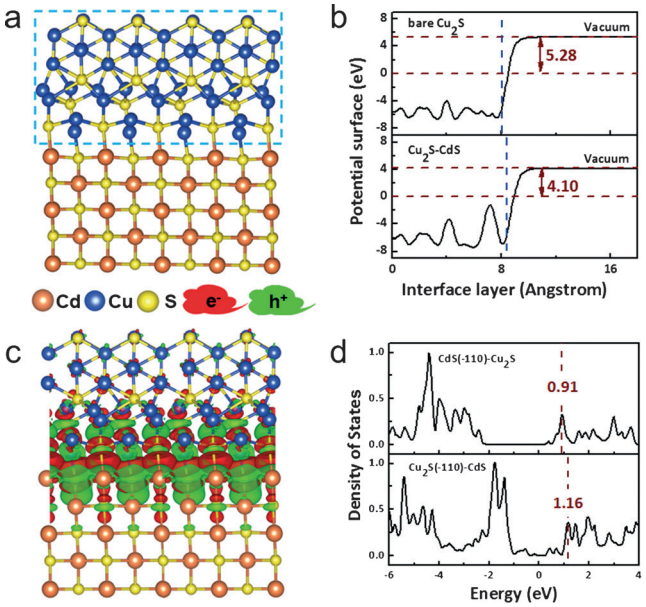

Figure 3. a) Atomic model of the interface of the CdS(−110)–Cu_2S(−110) heterostructure. b) The computed potential surfaces of the bare Cu_2S(−110) and Cu_2S(−110) fragments of the CdS(−110)–Cu_2S(−110) heterostructures, giving work functions of 5.28 and 4.10 eV, respectively. c) Simulated charge distribution at the CdS(−110)–Cu_2S(−110) interface. d) The computed partial densities of states (DOS) for the CdS and Cu_2S fragments at the CdS(−110)–Cu_2S(−110)interface.

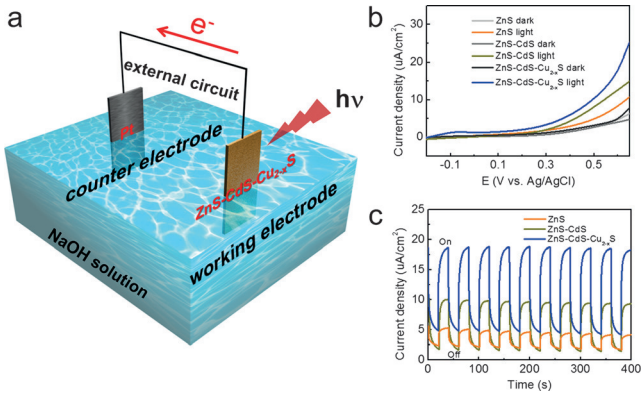

Figure 4. a) Schematic illustration of a photoelectrochemical water splitting cell. b) Linear sweep voltammetry (LSV) curves for three semiconductor photoanodes in the dark and under full-spectrum illumination; scan rate: 10 $mV s^{-1}$. c) Photoelectric response versus time (*J*–*t*) curves measured at 0.6 V vs. Ag/AgCl in 0.5 M NaOH electrolyte under chopped full-spectrum irradiation. All measurements were conducted under illumination with a 300 W Xe lamp with a light intensity of 100 $mW cm^{-2}$.

function of Cu_2S in the CdS(−110)/Cu_2S(−110) heterostructure had decreased by approximately 1.2 eV compared to that of bare Cu_2S(−110) (Figure 3b). Furthermore, Bader charge analysis indicated that CdS(−110) donates 0.11 electrons to Cu_2S(−110) (Figure 3c). These findings imply that the energy bands of Cu_2S(−110) might be levitated. By deducting the impurity states, the density of states of the CdS(−110)/Cu_2S(−110) heterostructure was calculated. We thus found that the conduction band of Cu_2S is approximately 0.3 eV higher in energy than that of CdS (Figure 3d). All of the above results suggest that this ternary system enables the separation of photogenerated carriers (Scheme S1).

To assess the effect of solar energy conversion by the ternary multi-node sheath ZnS–CdS–$Cu_{2-x}S$ heteronanorods, photocurrent measurements were utilized as a rough but useful method. CdS–$Cu_{2-x}S$ heterostructures that are formed by partial cation exchange from CdS frequently have Cu doping within the CdS region, which leads to a decrease in the excited-state lifetimes and poor photoconversion.[18] Thus, copper ion impurities in the ternary sulfide sample were selectively extracted by using tri-*n*-butylphosphine before the photocurrent tests (for details see the Supporting Information). To illustrate that the ternary ZnS–CdS–$Cu_{2-x}S$ heteronanorods utilize the full spectrum of solar irradiation, we employed a Xe lamp with a light intensity of 100 $mW cm^{-2}$ as the light source to achieve full-spectrum irradiation ($300 < \lambda < 2500$ nm) without any cutoff filters. A photoelectrochemical water splitting cell is shown in Figure 4a. Under solar light irradiation, the photogenerated electrons and holes will separate and flow to two electrode surfaces, with an applied potential promoting this process. The holes collected at the photoanode are used for the half-reaction of water oxidation into oxygen while the electrons collected at the Pt electrode enable the half-reaction of water reduction into hydrogen. The linear-sweep voltammetry curves in Figure 4b indicate an obvious increase in the photocurrent density after the integration of a visible-light absorption component (CdS) and a UV absorption component (ZnS), and further integration of an NIR absorption component ($Cu_{2-x}S$) to form pn junctions between CdS and $Cu_{2-x}S$. The enhancement in the photoelectric response after integration of $Cu_{2-x}S$ was further confirmed by the current–time (*J*–*t*) curves recorded at 0.6 V vs. Ag/AgCl in 0.5 M NaOH electrolyte under chopped full-spectrum irradiation (Figure 4c). The photocurrent was increased by a factor of greater than two by the incorporation of CdS (ca. 7.7 $\mu A cm^{-2}$) into ZnS (ca. 2.8 $\mu A cm^{-2}$), and the photocurrent of the ternary ZnS–CdS–$Cu_{2-x}S$ heteronanorods exceeded that of binary ZnS–CdS by a factor of 1.8 (ca. 14 $\mu A cm^{-2}$).

In conclusion, we have successfully synthesized ternary multi-node sheath sulfide ZnS–CdS–$Cu_{2-x}S$ heteronanorods by colloidal chemical transformations. These heteronanorods absorb across nearly the full spectrum of solar energy, including the UV (through ZnS), visible (through CdS), and NIR (through $Cu_{2-x}S$) range. The formation of nonstoichiometric copper sulfide ($Cu_{2-x}S$) provides free holes in the valence band, inducing LSPR effects and consequently achieving NIR absorption. In particular, the selective incorporation of $Cu_{2-x}S$ in CdS domains in our designed ternary heteronanorods results in a staggered gap alignment owing to the construction of pn heterojunctions. Such a staggered alignment enables the separation of the photogenerated electrons and holes in the ternary hybrid nanostructure. Photocurrent measurements, a simple but very useful test, demonstrated the enhancement of the charge-separation efficacy in the ternary ZnS–CdS–$Cu_{2-x}S$ heteronanosystem compared to binary ZnS–CdS and single ZnS. The multiple

selective integration of p-type and n-type sulfides that feature variable band gaps but do not contain any noble metals may provide a new approach for the development of semiconducting materials with enhanced full-spectrum solar energy absorption and efficient charge separation.

Acknowledgements

S.-H.Y. is grateful for funding from the National Natural Science Foundation of China (21431006), the Foundation for Innovative Research Groups of the National Natural Science Foundation of China (21521001), the National Basic Research Program of China (2014CB931800, 2013CB931800), the Users with Excellence and Scientific Research Grant of Hefei Science Center of CAS (2015HSC-UE007, 2015SRG-HSC038), and the Chinese Academy of Sciences (KJZD-EW-M01-1). T.-T.Z. acknowledges the China Postdoctoral Science Foundation (2015M582012).

Keywords: charge separation · heteronanorods · photocatalysis · solar energy conversion · ternary systems

How to cite: *Angew. Chem. Int. Ed.* **2016**, *55*, 6396–6400
Angew. Chem. **2016**, *128*, 6506–6510

[1] a) M. T. Mayer, Y. Lin, G. Yuan, D. Wang, *Acc. Chem. Res.* **2013**, *46*, 1558–1566; b) Z. C. Zhang, B. Xu, X. Wang, *Chem. Soc. Rev.* **2014**, *43*, 7870–7886; c) P. Zhang, T. Wang, J. L. Gong, *Adv. Mater.* **2015**, *27*, 5328–5342.

[2] a) J. Tang, Z. Huo, S. Brittman, H. Gao, P. Yang, *Nat. Nanotechnol.* **2011**, *6*, 568–572; b) B. S. Mashford, M. Stevenson, Z. Popovic, C. Hamilton, Z. Zhou, C. Breen, J. Steckel, V. Bulovic, M. Bawendi, S. Coe-Sullivan, *Nat. Photonics* **2013**, *7*, 407–412; c) X. Dai, Z. Zhang, Y. Jin, Y. Niu, H. Cao, X. Liang, L. Chen, J. Wang, X. Peng, *Nature* **2014**, *515*, 96–99.

[3] a) W. Gao, H. K. Lee, J. Hobley, T. Liu, I. Y. Phang, X. Y. Ling, *Angew. Chem. Int. Ed.* **2015**, *54*, 3993–3996; *Angew. Chem.* **2015**, *127*, 4065–4068; b) X. Sun, C. Wang, M. Gao, A. Hu, Z. Liu, *Adv. Funct. Mater.* **2015**, *25*, 2480.

[4] a) S. Cho, M. J. Lee, M. S. Kim, S. Lee, Y. K. Kim, D. H. Lee, C. W. Lee, K. H. Cho, J. H. Chung, *J. Dermatol. Sci.* **2008**, *50*, 123–133; b) J. Cui, Y. Li, L. Liu, L. Chen, J. Xu, J. Ma, G. Fang, E. Zhu, H. Wu, L. Zhao, *Nano Lett.* **2015**, *15*, 6295–6301.

[5] a) F. Capasso, *Science* **1987**, *235*, 172–176; b) A. M. Smith, S. Nie, *Acc. Chem. Res.* **2010**, *43*, 190–200; c) Y. Du, Z. Yin, J. Zhu, X. Huang, X.-J. Wu, Z. Zeng, Q. Yan, H. Zhang, *Nat. Commun.* **2012**, *3*, 1177–1183; d) M. R. Gao, Y. F. Xu, J. Jiang, S. H. Yu, *Chem. Soc. Rev.* **2013**, *42*, 2986–3017; e) X. J. Wu, X. Huang, X. Qi, H. Li, B. Li, H. Zhang, *Angew. Chem. Int. Ed.* **2014**, *53*, 8929–8933; *Angew. Chem.* **2014**, *126*, 9075–9079; f) G. Jia, U. Banin, *J. Am. Chem. Soc.* **2014**, *136*, 11121–11127; g) X. J. Wu, X. Huang, J. Liu, H. Li, J. Yang, B. Li, W. Huang, H. Zhang, *Angew. Chem. Int. Ed.* **2014**, *53*, 5083–5087; *Angew. Chem.* **2014**, *126*, 5183–5187; h) E. Lhuillier, S. Pedetti, S. Ithurria, B. Nadal, H. Heuclin, B. Dubertret, *Acc. Chem. Res.* **2015**, *48*, 22–30.

[6] a) Z. Wang, L. L. Daemen, Y. Zhao, C. S. Zha, R. T. Downs, X. Wang, Z. L. Wang, R. J. Hemley, *Nat. Mater.* **2005**, *4*, 922–927; b) X. Y. Wang, X. F. Ren, K. Kahen, M. A. Hahn, M. Rajeswaran, S. Maccagnano-Zacher, J. Silcox, G. E. Cragg, A. L. Efros, T. D. Krauss, *Nature* **2009**, *459*, 686–689; c) X. Fang, T. Zhai, U. K. Gautam, L. Li, L. Wu, Y. Bando, D. Golberg, *Prog. Mater. Sci.* **2011**, *56*, 175–287.

[7] a) J. Li, S. K. Cushing, P. Zheng, T. Senty, F. Meng, A. D. Bristow, A. Manivannan, N. Wu, *J. Am. Chem. Soc.* **2014**, *136*, 8438–8449; b) K. Wu, H. Zhu, Z. Liu, W. Rodríguez-Córdoba, T. Lian, *J. Am. Chem. Soc.* **2012**, *134*, 10337–10340; c) T. Simon, N. Bouchonville, M. J. Berr, A. Vaneski, A. Adrović, D. Volbers, R. Wyrwich, M. Döblinger, A. S. Susha, A. L. Rogach, F. Jäckel, J. K. Stolarczyk, J. Feldmann, *Nat. Mater.* **2014**, *13*, 1013–1018; d) T. Wang, J. Zhuang, J. Lynch, O. Chen, Z. Wang, X. Wang, D. LaMontagne, H. Wu, Z. Wang, Y. C. Cao, *Science* **2012**, *338*, 358–363.

[8] T. T. Zhuang, Y. Liu, M. Sun, S. L. Jiang, M. W. Zhang, X. C. Wang, Q. Zhang, J. Jiang, S. H. Yu, *Angew. Chem. Int. Ed.* **2015**, *54*, 11495–11500; *Angew. Chem.* **2015**, *127*, 11657–11662.

[9] a) Y. Zhao, H. Pan, Y. Lou, X. Qiu, J. Zhu, C. Burda, *J. Am. Chem. Soc.* **2009**, *131*, 4253–4261; b) S.-W. Hsu, W. Bryks, A. R. Tao, *Chem. Mater.* **2012**, *24*, 3765–3771; c) X. Wang, Y. Ke, H. Pan, K. Ma, Q. Xiao, D. Yin, G. Wu, M. T. Swihart, *ACS Catal.* **2015**, *5*, 2534–2540.

[10] a) J. Zhang, Y. Tang, K. Lee, M. Ouyang, *Nature* **2010**, *466*, 91–95; b) K. Wu, H. Zhu, T. Lian, *Acc. Chem. Res.* **2015**, *48*, 851–859; c) K. Wu, J. Chen, J. R. McBride, T. Lian, *Science* **2015**, *349*, 632–635.

[11] a) A. Nayak, T. Ohno, T. Tsuruoka, K. Terabe, T. Hasegawa, J. K. Gimzewski, M. Aono, *Adv. Funct. Mater.* **2012**, *22*, 3606–3613; b) W. Bryks, M. Wette, N. Velez, S.-W. Hsu, A. R. Tao, *J. Am. Chem. Soc.* **2014**, *136*, 6175–6178.

[12] A. B. Wong, S. Brittman, Y. Yu, N. P. Dasgupta, P. D. Yang, *Nano Lett.* **2015**, *15*, 4096–4101.

[13] a) D. H. Son, S. M. Hughes, Y. Yin, A. P. Alivisatos, *Science* **2004**, *306*, 1009–1012; b) R. D. Robinson, B. Sadtler, D. O. Demchenko, C. K. Erdonmez, L.-W. Wang, A. P. Alivisatos, *Science* **2007**, *317*, 355–358.

[14] B. J. Beberwyck, Y. Surendranath, A. P. Alivisatos, *J. Phys. Chem. C* **2013**, *117*, 19759–19770.

[15] H. Li, M. Zanella, A. Genovese, M. Povia, A. Falqui, C. Giannini, L. Manna, *Nano Lett.* **2011**, *11*, 4964–4970.

[16] M. Hu, G. V. Hartland, *J. Phys. Chem. B* **2002**, *106*, 7029–7033.

[17] S. W. Goh, A. N. Buckley, R. N. Lamb, R. A. Rosenberg, D. Moran, *Geochim. Cosmochim. Acta* **2006**, *70*, 2210–2218.

[18] I. Jen-La Plante, A. Teitelboim, I. Pinkas, D. Oron, T. Mokari, *J. Phys. Chem. Lett.* **2014**, *5*, 590–596.

Received: February 23, 2016
Published online: April 9, 2016

